LETTERS
PUBLISHED ONLINE: 22 APRIL 2012 | DOI: 10.1038/NMAT3303
nature materials

Effects of chemical bonding on heat transport across interfaces

Mark D. Losego[1,2]*, Martha E. Grady[2,3], Nancy R. Sottos[1,2,3], David G. Cahill[1,3] and Paul V. Braun[1,2]

Interfaces often dictate heat flow in micro- and nanostructured systems[1–3]. However, despite the growing importance of thermal management in micro- and nanoscale devices[4–6], a unified understanding of the atomic-scale structural features contributing to interfacial heat transport does not exist. Herein, we experimentally demonstrate a link between interfacial bonding character and thermal conductance at the atomic level. Our experimental system consists of a gold film transfer-printed to a self-assembled monolayer (SAM) with systematically varied termination chemistries. Using a combination of ultrafast pump–probe techniques (time-domain thermoreflectance, TDTR, and picosecond acoustics) and laser spallation experiments, we independently measure and correlate changes in bonding strength and heat flow at the gold–SAM interface. For example, we experimentally demonstrate that varying the density of covalent bonds within this single bonding layer modulates both interfacial stiffness and interfacial thermal conductance. We believe that this experimental system will enable future quantification of other interfacial phenomena and will be a critical tool to stimulate and validate new theories describing the mechanisms of interfacial heat transport. Ultimately, these findings will impact applications, including thermoelectric energy harvesting, microelectronics cooling, and spatial targeting for hyperthermal therapeutics.

Thermal conductivity (λ) relates the heat flux (Q) to the temperature gradient (∇T) in a bulk material through Fourier's law ($\lambda = Q/\nabla T$). Similarly, interfacial thermal conductance (G) defines the finite temperature drop (ΔT) for a given heat flux across an interface ($G = Q/\Delta T$). Whereas at macroscopic length-scales λ controls heat flow, heat transport in nanostructured materials systems is strongly influenced or even dominated by G (refs 1–3). For electrically insulating interfaces where thermal transport occurs only via lattice vibrations (phonons), G has generally been predicted using either the acoustic mismatch model (AMM; ref. 7) or the diffuse mismatch model (DMM; ref. 8). Both models derive phonon transmission probabilities from bulk material properties. The AMM uses differences in acoustic impedance whereas the DMM uses differences in the phonon density of states. Both lack parameters that account for differences in atomic-scale interfacial structure. This simplifying assumption makes these models unreliable at predicting G for real interfaces. Experimental work by Hopkins *et al.*[9] demonstrated that increasing the interfacial roughness lowers the value of G of an Al/Si interface by ~15%. Molecular dynamics (MD) simulations[10–12] as well as analytical models[13] predict interfacial bond strength can cause G to vary by an order of magnitude. Here, we create an experimental system where interfacial bonding chemistry is systematically varied to study the correlation between bonding character and thermal conductance.

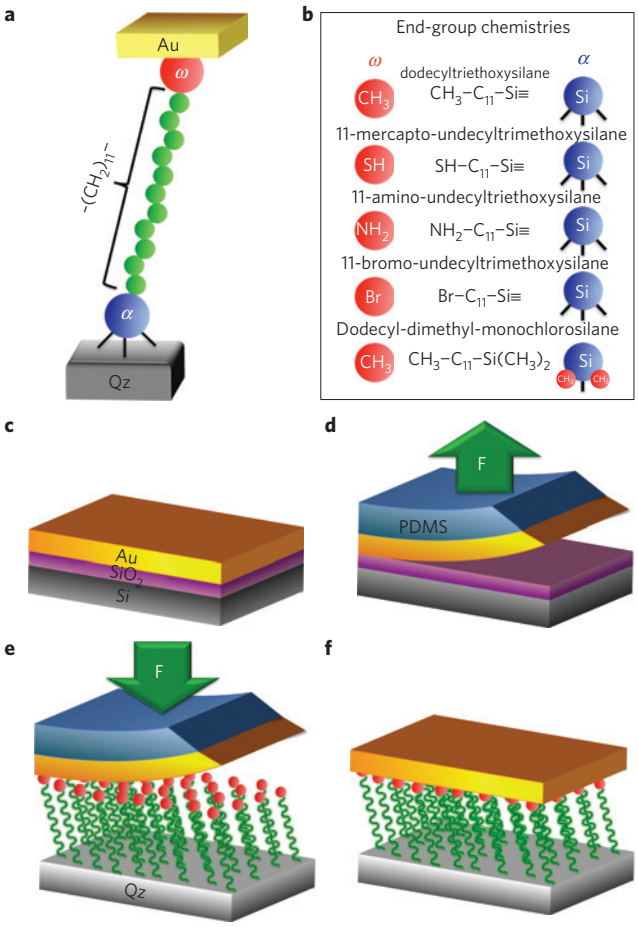

Figure 1 | Experimental system. a, Depiction of the experimental system consisting of a Qz substrate, bifunctional SAM, and transfer-printed Au layer. **b**, List of all SAM chemistries studied and abbreviations used in the text. **c**–**f**, Schematic of the transfer printing process: deposition of Au on a donor substrate (**c**); PDMS stamp used to remove gold film (**d**); printing of gold film on SAM/Qz surface (**e**); final test structure (**f**).

To achieve an interface with variable bonding chemistry, we use self-assembled monolayers (SAMs) sandwiched between a z-cut quartz (Qz) substrate and a transfer-printed gold (Au) film[14]. By varying the SAM's end-group functionalities (illustrated in

[1]Department of Materials Science and Engineering, Frederick Seitz Materials Research Laboratory, University of Illinois at Urbana-Champaign, Urbana, Illinois 61801, USA, [2]Beckman Institute for Advanced Science and Technology, University of Illinois at Urbana-Champaign, Urbana, Illinois 61801, USA, [3]Department of Mechanical Science and Engineering, University of Illinois at Urbana-Champaign, Urbana, Illinois 61801, USA.
*e-mail: marklosego@gmail.com.

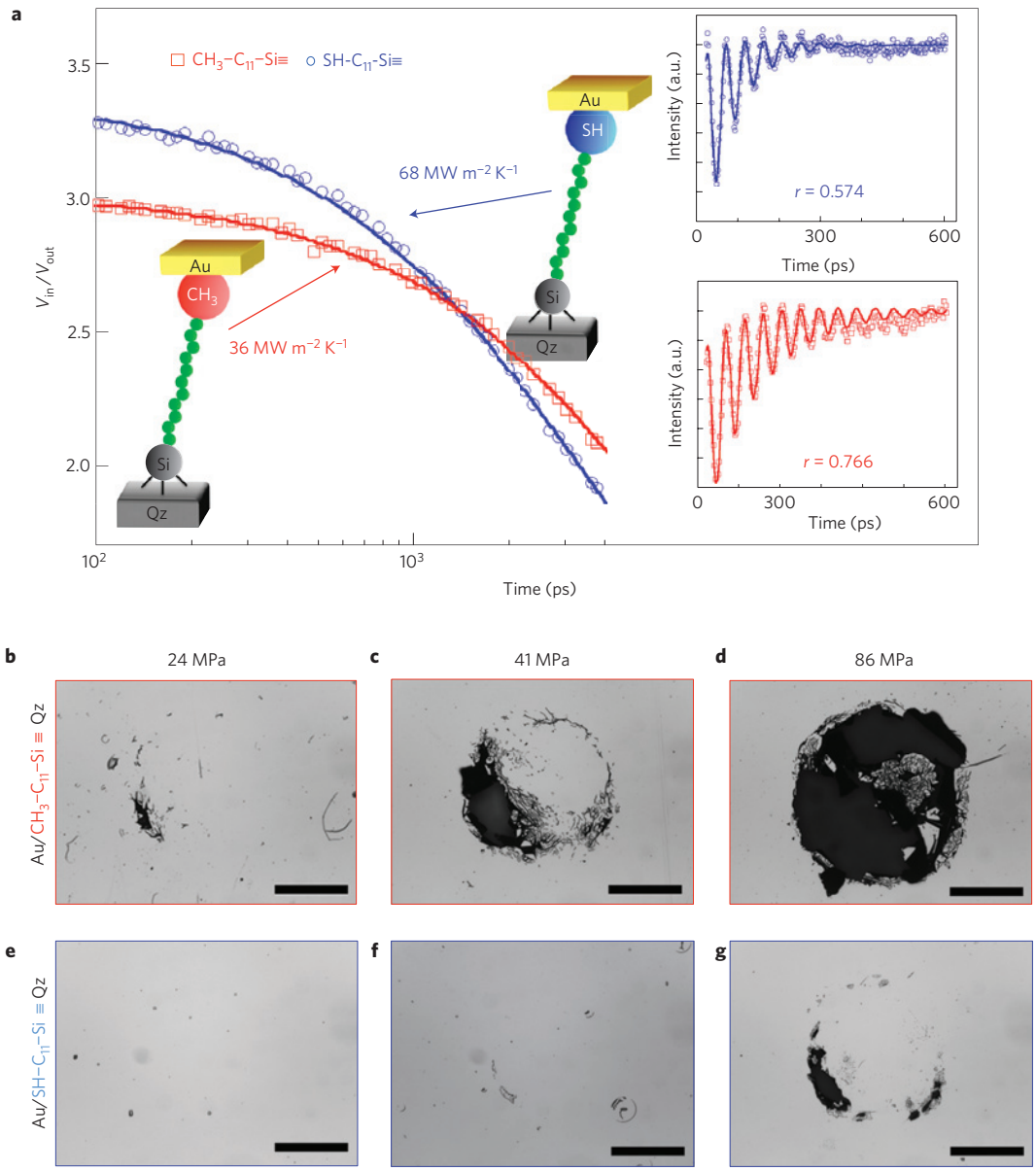

Figure 2 | Correlation between interfacial thermal transport and bond strength. a, TDTR thermal transport measurements (symbols) along with fits (lines) for representative Au/CH_3-C_{11}-Si≡Qz and Au/SH-C_{11}-Si≡Qz structures. Inset shows picosecond acoustic data collected from an offset pump–probe beam geometry, for representative Au/CH_3-C_{11}-Si≡Qz (bottom) and Au/SH-C_{11}-Si≡Qz (top) structures with the extracted acoustic reflectance value shown (see Supplementary Information for data analysis details). **b**–**g**, Optical images of delamination damage (black areas) caused by laser spallation to Au/CH_3-C_{11}-Si interfaces (**b**–**d**) and Au/SH-C_{11}-Si interfaces (**e**–**g**) at increasing stress amplitudes: (**b**,**e**) 24 MPa, (**c**,**f**) 41 MPa, (**d**,**g**) 86 MPa. Scale bars are 500 μm.

Fig. 1a,b) we control the bond strength across the interface. We choose the Au/Qz interface because bifunctional molecules with orthogonal attachment chemistries having specificity towards either Qz or Au can be used. Silane chemistries on the α-end permit dense packing and strong bonding of the molecules to the Qz surface. Diverse ω-end-group chemistries (for example $-CH_3$, $-SH$) permit large variations in bond strength at the Au/SAM interface. When properly formed, these chemistries result neither in multilayer formation nor loop attachment to the Qz substrate (see Supplementary Information).

As illustrated in Fig. 1c–f, gold films are removed from SiO_2 donor substrates (thermally grown on silicon) using a polydimethylsiloxane (PDMS) elastomer stamp (Sylgard 184, Dow Corning) and laminated onto SAM-functionalized Qz substrates under modest pressure and temperature (120 °C). This process is known as 'transfer-printing'. Taking advantage of the viscoelastic nature of the PDMS stamp, a slow peel velocity releases the gold film onto the receiving surface independent of its surface chemistry (Supplementary Fig. S1)[14]. Thus, Au films can be transfer-printed to surface chemistries expected to give both strong covalent bonds (for example $-SH$) as well as weak van der Waals attractions (for example $-CH_3$, clean Qz). Previous work in molecular electronics[15] has demonstrated that this 'soft-deposition' approach of transfer-printing (as compared with more energetic physical vapour deposition techniques) causes minimal damage to the SAM layer. Thus, we expect the transfer-printed gold layer to be in direct contact with the selected end-group chemistry, permitting examination of the effects of a single bonding layer on interfacial heat transport.

The thermal conductance in these Au/SAM/Qz systems is measured by time-domain thermoreflectance (TDTR), which is

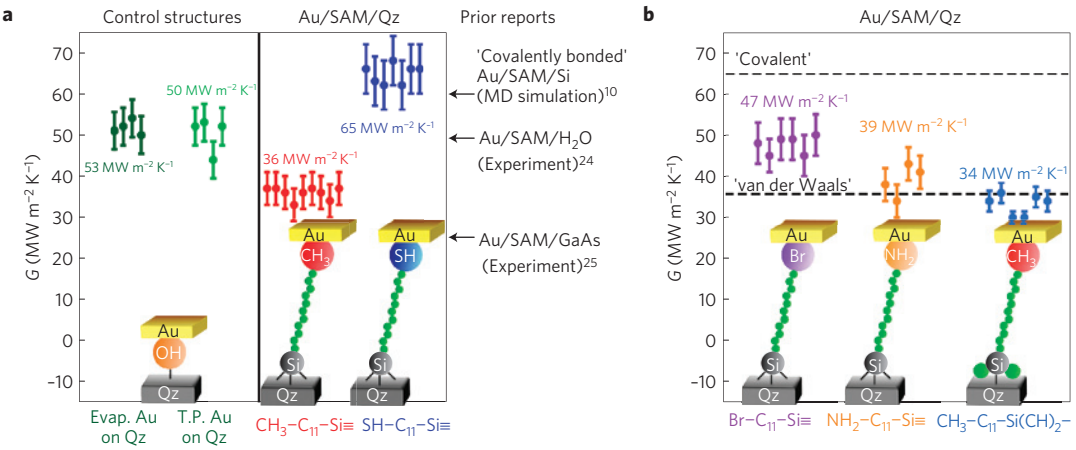

Figure 3 | Interfacial thermal conductance for varying chemistries. Interfacial thermal conductance values (G) measured for multiple, independently prepared structures of each interfacial chemistry, depicted below data points. **a**, Control structures consist of gold evaporated on Qz and gold transfer-printed (TP) to Qz. Experimental structures consist of Au/CH_3–C_{11}–Si≡Qz and Au/SH–C_{11}–Si≡Qz. Related reports of previously published data are highlighted with arrows on the right. **b**, Interfacial thermal conductance measured for other interfacial chemistries including Au/Br–C_{11}–Si≡Qz, Au/NH_2–C_{11}–Si≡Qz, and Au/CH_3–C_{11}–Si$(CH_3)_2$–Qz. Error bars represent uncertainty in TDTR data fitting (see Supplementary Information for details).

an optical measurement technique using an ultrafast pump–probe arrangement[16,17]. In this measurement, a mode-locked laser is split into two pulsed beams. The pump pulses are of high intensity and are absorbed by the metal layer, creating a temperature rise. The probe pulses monitor the surface temperature by means of thermoreflectance as a function of time after the initial heating pulse. Because TDTR uses a mode-locked laser with picosecond pulse widths, nanoscale depth resolution is obtained in the thermal conductance measurement. Unlike other techniques, the nanoscale depth resolution of TDTR permits the interfacial thermal conductance to be separated from the bulk thermal conductance of each layer[4,16].

As a simple example, we first examine heat transport at Au/SAM/Qz interfaces using SAMs of the same length and different ω-end-groups: (1) methyl (CH_3–C_{11}–Si≡) and (2) thiol (SH–C_{11}–Si≡). We expect the thiol functionality to form a strong covalent-like bond to the gold film[18,19] whereas only a weak van der Waals attraction should attach the gold film to the methyl-terminated surface. Figure 2a plots representative TDTR data comparing the thermal transport properties in both systems. To a first approximation, these plots represent the change in the gold surface temperature as a function of time after the initial laser heating pulse. Evident in this figure is the much faster temperature decay observed for the Au/thiol interface than the Au/methyl interface. To quantify this effect, we fit the data to a thermal diffusion model[17]. By independently measuring all other relevant parameters in this thermal diffusion model, we extract the interfacial thermal conductance (G) from the data (see Supplementary Information for details of experimental measurements). For the data presented in Fig. 2, we find $G = 68\ \mathrm{MW\,m^{-2}\,K^{-1}}$ for the Au/SH–C_{11}–Si≡Qz interface and $G = 36\ \mathrm{MW\,m^{-2}\,K^{-1}}$ for the Au/CH_3–C_{11}–Si≡Qz interface, confirming that interfacial bonding directly impacts thermal conductance.

Although covalent-like bonding is generally believed to occur between thiols and Au surfaces, we desire independent experimental measurements of the bonding character at the Au/SAM/Qz interfaces to unequivocally verify the correlation between interfacial bonding and heat transport. We first use picosecond acoustics to investigate interfacial bond stiffness, as shown in the inset of Fig. 2a (see Supplementary Information for experimental details). The damping rate of this longitudinal wave describes how well acoustic energy is coupled across the interface and can be used to calculate an interfacial stiffness[20,21]. Quicker damping of the acoustic signal indicates higher acoustic transmission across the Au/SAM interface at the system's normal mode frequency. We find that the acoustic reflectance of the Au/SH–C_{11}–Si≡Qz interface ($r = 0.574$) matches that of an 'ideally bonded' AMM interface ($r = 0.577$) at these vibrational frequencies (~22 GHz). Unfortunately, because of this high bond strength, we cannot quantify interfacial stiffness using these low vibrational frequencies. The Au/CH_3–C_{11}–Si≡Qz interface has much higher reflectivity ($r = 0.766$), implying less clamping at the interface and allowing us to calculate a value for the interfacial stiffness ($2.7 \times 10^{14}\ \mathrm{N\,m^{-3}}$). From these measurements, we can directly conclude that interfacial bonding in the Au/SH–C_{11}–Si≡Qz system is substantially stiffer than in the Au/CH_3–C_{11}–Si≡Qz system.

Laser-induced spallation experiments[22,23] are used to characterize the macroscopic adhesion strength of the transfer-printed Au layers. In these experiments a pulsed Nd:YAG laser generates a high-amplitude longitudinal stress wave on the backside of the substrate. On reflection from the Au surface, this stress wave loads the Au film in tension, effectively testing its adhesion strength (Supplementary Fig. S10). By making multiple measurements at increased stress amplitudes (controlled by the laser fluence), the adhesion strengths of Au layers transfer-printed to different SAM chemistries can be compared. Figure 2b–g shows representative images of Au films after laser-induced adhesion tests. Qualitatively, we observe that delamination failure of the Au/CH_3–C_{11}–Si≡Qz structures consistently occurs at significantly lower stress amplitudes than the Au/SH–C_{11}–Si≡Qz structures. The size of the damaged area is also much larger for the Au/CH_3–C_{11}–Si≡Qz structures when compared at the same stress amplitude. We calculate a spallation strength of 24.2 ± 0.4 MPa for Au/CH_3–C_{11}–Si≡Qz and 60 ± 11 MPa for Au/SH–C_{11}–Si≡Qz, confirming that interfacial bonding at the Au/thiol interface is significantly stronger than at the Au/methyl interface (see Supplementary Information for details).

We next turn to verifying the reproducibility and validity of our thermal measurements. Figure 3a summarizes values for G measured from independently prepared Au/SAM/Qz structures and places them in context with previous studies[10,24,25]. These data demonstrate the repeatability of our process. Measurements made on control structures consisting of Au evaporated on Qz and Au transfer-printed to Qz show remarkably similar thermal transport behaviour, indicating that the quality of the transfer-printed interfaces is equivalent to standard thin-film deposition procedures. From these results, we conclude that our combined

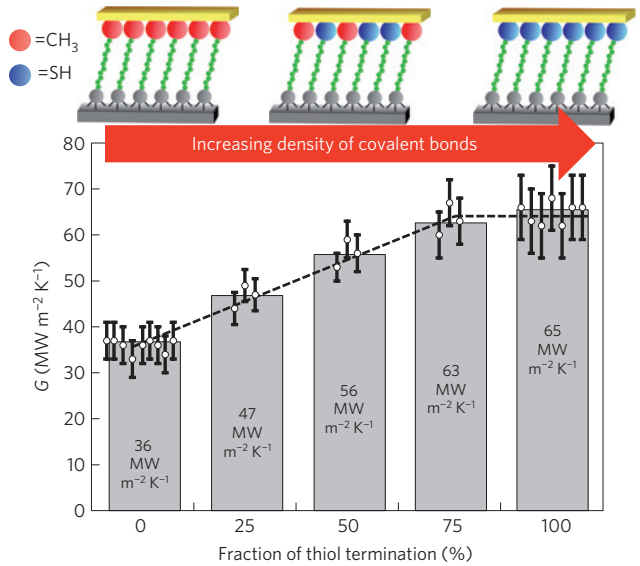

Figure 4 | Tuning interfacial thermal conductance. Plot of interfacial thermal conductance (G) as a function of the methyl:thiol end-group ratio for 0%, 25%, 50%, 75% and 100% thiol end groups. Duplicated structures for each ratio were measured. Error bars represent uncertainty in TDTR data fitting (see Supplementary Information for details).

transfer-printing/TDTR set-up can accurately probe the thermal conductance across a molecular interface. Our measurements for G also show good agreement with previous reports of thermal transport across SAM interfaces[10,24–26]. Particularly striking is the similarity between G measured for Au/SH–C_{11}–Si≡Qz ($G_{avg} = 65\,MW\,m^{-2}\,K^{-1}$) and the recent calculations by Keblinski and colleagues for a Au/SAM/Si interface with strong bonding at both SAM end-groups ($G = 60\,MW\,m^{-2}\,K^{-1}$; ref. 10).

To further explore the importance of a single bonding layer on heat transfer, we investigate the thermal transport across Au/SAM/Qz interfaces using other ω-end-group and α-attachment chemistries but having the same methylene chain length (Fig. 3b). Approximate boundary lines are drawn representing van der Waals ($36\,MW\,m^{-2}\,K^{-1}$) and covalent ($65\,MW\,m^{-2}\,K^{-1}$) bonding in our system based on the average measurements for the Au/CH_3–C_{11}–Si≡Qz and Au/SH–C_{11}–Si≡Qz structures respectively. Surprisingly, G for the amine-terminated surface is roughly equivalent to the methyl-terminated surface. Although charged quaternary amines bind strongly to Au, particularly when used as stabilizing ligands for Au nanoparticles[27], the primary amine-Au binding energy in the dry, uncharged state is calculated to be only ~0.25 eV (ref. 28), about 5× less than the Au–S bond energy (~1.4 eV; ref. 19). The low surface roughness of the gold may also contribute to weaker binding, as amines are believed to bond more strongly to under-coordinated Au adatom defects[29]. Bromine-terminated surfaces give a higher interfacial thermal conductance ($G_{avg} = 47\,MW\,m^{-2}\,K^{-1}$) than a van der Waals interaction. We offer two possible explanations: (1) the high electron-density from the three sets of lone-pair electrons generates a stronger van der Waals interaction at this interface or (2) the heavier bromine moiety has a better vibrational match to the heat-conducting phonons in gold, permitting more effective coupling. Dodecyl SAMs formed using a dimethylmonochlorosilane attachment chemistry are found to have a thermal conductance that is effectively lower than the van der Waals limit. However, experimental characterization of these SAMs reveals a lower surface coverage than the tri-functional silanes. Thus, the reduction in G is believed to be a consequence of having a lower density monolayer[30].

Finally, we demonstrate the ability to directly tune the interfacial thermal conductance. In this experiment, the Au/SAM/Qz structures are formed using mixed monolayers of SH–C_{11}–Si≡ and CH_3–C_{11}–Si≡. (See Supplementary Fig. S5 for X-ray photoelectron spectroscopy analysis.) Measurements of G for these mixed monolayers are shown in Fig. 4. Apparent in this figure is a monotonic increase in G with increased SH–C_{11}–Si≡ concentration up to 75% SH–C_{11}–Si≡. This result implies that as the number of covalent (Au–thiol) attachment sites increases, phonons couple more strongly across the interface. A plateau in G is reached for a concentration of 75% SH–C_{11}–Si≡. This plateau effect with interfacial bond strength is consistent with MD simulations made for silicon/polyethylene interfaces[12] and water/SAM interfaces[11]. Mechanistically, at some critical bond strength, the 'spring constant' between the two materials becomes stiff enough to effectively couple all relevant heat-carrying phonon frequencies across the interface. At this point, other factors, such as acoustic mismatch, differences in the phonon density of states, or interfacial roughness limit heat transport across the interface.

In summary, we have experimentally shown that the strength of a single bonding layer directly controls phonon heat transport across an interface. Although transitioning from van der Waals to covalent bonding increases G by ~80% for Au/Qz interfaces, it is possible that much greater contrast could be achieved in systems that have more similarity in their vibrational properties (refs 12,13). More importantly, this experimental system provides a simple route to probing vibrational transport phenomena across interfaces. We expect future experiments using similar techniques combined with theoretical calculations will lead to a clearer fundamental description of interfacial thermal conductance and reveal new opportunities for engineering heat transport in nanostructured systems.

Methods

Detailed descriptions of SAM deposition and characterization, transfer printing procedures, TDTR measurements, picosecond acoustic measurements, laser spallation measurements and data analysis are provided in the Supplementary Information.

Received 9 December 2011; accepted 15 March 2012; published online 22 April 2012

References

1. Losego, M. D., Moh, L., Arpin, K. A., Cahill, D. G. & Braun, P. V. Interfacial thermal conductance in spun-cast polymer films and polymer brushes. *Appl. Phys. Lett.* **97,** 011908 (2010).
2. Hung, M. T., Choi, O., Ju, Y. S. & Hahn, H. T. Heat conduction in graphite-nanoplatelet-reinforced polymer nanocomposites. *Appl. Phys. Lett.* **89,** 023117 (2006).
3. Chiritescu, C. *et al.* Ultralow thermal conductivity in disordered, layered WSe2 crystals. *Science* **315,** 351–353 (2007).
4. Cahill, D. G. *et al.* Nanoscale thermal transport. *J. Appl. Phys.* **93,** 793–818 (2003).
5. Garimella, S. V. Advances in mesoscale thermal management technologies for microelectronics. *Microelectron. J.* **37,** 1165–1185 (2006).
6. Bae, M. H., Ong, Z. Y., Estrada, D. & Pop, E. Imaging, simulation, and electrostatic control of power dissipation in graphene devices. *Nano Lett.* **10,** 4787–4793 (2010).
7. Little, W. A. The transport of heat between dissimilar solids at low temperatures. *Can. J. Phys.* **37,** 334–349 (1959).
8. Swartz, E. T. & Pohl, R. O. Thermal-boundary resistance. *Rev. Mod. Phys.* **61,** 605–668 (1989).
9. Hopkins, P. E., Phinney, L. M., Serrano, J. R. & Beechem, T. E. Effects of surface roughness and oxide layer on the thermal boundary conductance at aluminum/silicon interfaces. *Phys. Rev. B* **82,** 085307 (2010).
10. Hu, L. *et al.* Phonon interference at self-assembled monolayer interfaces: Molecular dynamics simulations. *Phys. Rev. B* **81,** 235427 (2010).
11. Shenogina, N., Godawat, R., Keblinski, P. & Garde, S. How wetting and adhesion affect thermal conductance of a range of hydrophobic to hydrophilic aqueous interfaces. *Phys. Rev. Lett.* **102,** 156101 (2009).
12. Hu, M., Keblinski, P. & Schelling, P. K. Kapitza conductance of silicon-amorphous polyethylene interfaces by molecular dynamics simulations. *Phys. Rev. B* **79,** 104305 (2009).

13. Prasher, R. Acoustic mismatch model for thermal contact resistance of van der Waals contacts. *Appl. Phys. Lett.* **94,** 041905 (2009).
14. Meitl, M. A. *et al.* Transfer printing by kinetic control of adhesion to an elastomeric stamp. *Nature Mater.* **5,** 33–38 (2006).
15. Loo, Y. L., Lang, D. V., Rogers, J. A. & Hsu, J. W. P. Electrical contacts to molecular layers by nanotransfer printing. *Nano Lett.* **3,** 913–917 (2003).
16. Cahill, D. G., Goodson, K. & Majumdar, A. Thermometry and thermal transport in micro/nanoscale solid-state devices and structures. *J. Heat Transfer* **124,** 223–241 (2002).
17. Cahill, D. G. Analysis of heat flow in layered structures for time-domain thermoreflectance. *Rev. Sci. Instrum.* **75,** 5119–5122 (2004).
18. Bain, C. D. *et al.* Formation of monolayer films by the spontaneous assembly of organic thiols from solution onto gold. *J. Am. Chem. Soc.* **111,** 321–335 (1989).
19. Yourdshahyan, Y. & Rappe, A. M. Structure and energetics of alkanethiol adsorption on the Au(111) surface. *J. Chem. Phys.* **117,** 825–833 (2002).
20. Tas, G., Loomis, J. J., Maris, H. J., Bailes, A. A. & Seiberling, L. E. Picosecond ultrasonics study of the modification of interfacial bonding by ion implantation. *Appl. Phys. Lett.* **72,** 2235–2237 (1998).
21. Antonelli, G. A., Perrin, B., Daly, B. C. & Cahill, D. G. Characterization of mechanical and thermal properties using ultrafast optical metrology. *Mater. Res. Sci. Bull.* **31,** 607–613 (2006).
22. Wang, J., Sottos, N. R. & Weaver, R. L. Mixed-mode failure of thin films using laser-generated shear waves. *Exp. Mech.* **43,** 323–330 (2003).
23. Wang, J. L., Weaver, R. L. & Sottos, N. R. Laser-induced decompression shock development in fused silica. *J. Appl. Phys.* **93,** 9529–9536 (2003).
24. Ge, Z. B., Cahill, D. G. & Braun, P. V. Thermal conductance of hydrophilic and hydrophobic interfaces. *Phys. Rev. Lett.* **96,** 186101 (2006).
25. Wang, R. Y., Segalman, R. A. & Majumdar, A. Room temperature thermal conductance of alkanedithiol self-assembled monolayers. *Appl. Phys. Lett.* **89,** 173113 (2006).
26. Wang, Z. H. *et al.* Ultrafast flash thermal conductance of molecular chains. *Science* **317,** 787–790 (2007).
27. Feng, J. *et al.* Adsorption mechanism of single amino acid and surfactant molecules to Au{111} surfaces in aqueous solution: Design rules for metal-binding molecules. *Soft Matter* **7,** 2113–2120 (2011).
28. Hoft, R. C., Ford, M. J., McDonagh, A. M. & Cortie, M. B. Adsorption of amine compounds on the Au(111) surface: A density functional study. *J. Phys. Chem. B* **111,** 13886–13891 (2007).
29. Venkataraman, L. *et al.* Single-molecule circuits with well-defined molecular conductance. *Nano Lett.* **6,** 458–462 (2006).
30. Luo, T. F. & Lloyd, J. R. Equilibrium molecular dynamics study of lattice thermal conductivity/conductance of Au–SAM–Au junctions. *J. Heat Transfer* **132,** 032401 (2010).

Acknowledgements

We thank S. Dunham for helping to develop our transfer-printing process. This work is supported by the Air Force Office of Scientific Research (AFOSR) MURI FA9550-08-1-0407. N.R.S. acknowledges support from the National Science Foundation (NSF) CMMI 07-26742 and M.E.G. is supported by a Semiconductor Research Corporation (SRC) graduate fellowship. Fabrication and characterization were carried out in part in the Frederick Seitz Materials Research Laboratory at the University of Illinois at Urbana-Champaign, which is partially supported by the US Department of Energy under grants DE-FG02-07ER46453 and DE-FG02-07ER46471.

Author contributions

M.D.L. designed the experimental system with input from P.V.B. and D.G.C. M.D.L. made all the structures, characterized SAMs, conducted TDTR measurements and analysis, and wrote the paper. Picosecond acoustic measurements and analysis methodology were developed by M.D.L. with help from D.G.C. M.E.G. performed laser spallation measurements and adhesion analysis with input from N.R.S. All authors discussed data and commented on the manuscript.

Additional information

The authors declare no competing financial interests. Supplementary information accompanies this paper on www.nature.com/naturematerials. Reprints and permissions information is available online at www.nature.com/reprints. Correspondence and requests for materials should be addressed to M.D.L.